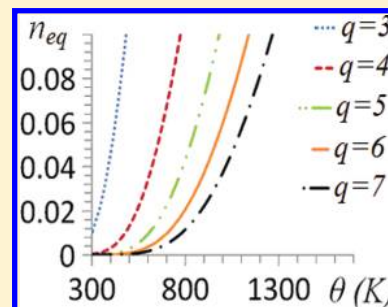


Mechanochemical Continuum Modeling of Nanovoid Nucleation and Growth in Reacting Nanoparticles

Valery I. Levitas^{*,†,‡,§} and Hamed Attariani^{‡,||}[†]Department of Aerospace Engineering, [‡]Department of Mechanical Engineering, and [§]Department of Material Science and Engineering, Iowa State University, Ames, Iowa 50011, United States

ABSTRACT: Hollow nanoparticles (NPs) are produced by void nucleation and growth during chemical reactions. However, there is no proper understanding of nucleation and growth mechanisms and their predictive modeling. Models based on the Kirkendall effect predict the process time, which is larger by orders of magnitude than in experiment. This is why some works propose that a large tensile pressure in the core causes void nucleation. Here, a continuum-mechanics approach for nucleation and growth of a nanovoid in reacting NPs based on the Kirkendall effect is developed. In contrast to previous approaches, void nucleation and the effects of stresses are treated explicitly. The void nucleation condition vs pressure, temperature, size of a vacancy, core material, and initial reaction product layer is determined, and a strong multifaceted effect of mechanics is revealed. Thus, with mechanics, a cluster consisting of four vacancies represents the supercritical nucleus. Surprisingly, the core is under compression (which eliminates fracture hypothesis), and compressive pressure and reduced temperature promote void nucleation by decreasing the equilibrium concentration of vacancies at the void surface. However, they suppress void growth by reducing the diffusion coefficients. Our model quantitatively describes the experimental results for oxidation of copper NPs. A thermomechanical loading program is suggested to accelerate and control void nucleation and growth.



INTRODUCTION

Hollow nanoparticles (NPs) have diverse functionality due to their specific optical, electrical, magnetic, and other properties. They have low density, high specific surface area, and the ability to encompass another material in their internal volume. These characteristics make them an outstanding candidate in biomedical applications (drug delivery, disease diagnosis, and cancer therapy), lightweight filters, composites, catalysts, waste treatment, insulators, and photoelectric devices.^{1,2} The hollow in nanoparticles can be used to control their energetic behavior during combustion.³ Understanding the mechanisms and parameters that affect hollow formation is a key issue for researchers. After the first synthesis of hollow nanoparticles⁴ based on the Kirkendall effect, experimental studies have been done on void formation in Cu, Al, Fe, Zn, Co, and Cd NPs.^{5–11} In studies described in refs 4–9, the bare NP was exposed to the air to cause oxidation; hollow sulfides were formed in the studies described in refs 10 and 11. Since diffusion of the core material to the oxide shell is faster than diffusion of oxide into the metal core (the Kirkendall effect¹²), vacancy flux to the core leads to an oversaturated vacancy state and nanovoid nucleation. While atomistic studies for model binary metals reproduce nucleation and growth of a void,^{13,14} due to a known limitation on the size and time scales, void nucleation was obtained near melting temperature only, while in experiments it occurs near room temperature. With the continuum approach, diffusional growth of a nanovoid in a binary alloy without reaction was studied for cylindrical¹⁵ and spherical^{16,17} particles. In all continuum approaches, nucleation

of the void was not considered, and the mechanics was neglected. Because the calculated growth time was larger by several orders of magnitude than in experiments,¹⁷ the ability to explain void formation by the Kirkendall effect was doubted. It is proposed in ref 17 that tensile pressure in the core is developed due to misfit strain between the metal and oxide, and that causes void nucleation. In ref 18, nucleation of the nanovoid caused by tensile stresses due to misfit strain was considered without diffusion. However, refs 17 and 18 neglect surface tension and stresses, which in fact produce large compressive pressure in a core (see below). Void nucleation in elastoplastic material under tensile stresses due to sublimation, sublimation via virtual melting, and fracture are considered in refs 19–21. In phase-field approaches,^{22,23} void nucleation occurs via spinodal decomposition for a very large concentration of vacancies or due to cavitation;²⁴ the results^{19–24} are not applicable to our case. Thus, the mechanism of void nucleation and growth is currently not clear. In this study, we developed a simple continuum approach for nucleation and growth of a nanovoid in reacted NPs that includes consideration of coupled core material reaction, diffusion of vacancies, diffusion of the core material in the reaction product shell, stress generation, and moving void and external surfaces. While equations are formulated for the general 3-D case, to obtain a simple and tractable solution, we consider a

Received: June 13, 2011

Revised: November 30, 2011

Published: December 28, 2011

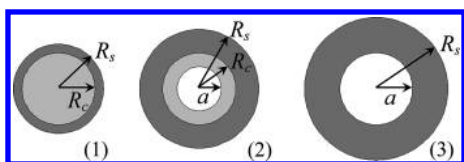


Figure 1. Particle geometry: (1) before void nucleation, (2) with all three regions, (3) after the metal core disappeared.

spherically symmetric problem. It is assumed that a q -vacancy cluster is formed at the center of a particle, which is considered as a void embryo. The concentration of vacancies at the void is equal to the thermodynamic equilibrium value n_{eq} , which depends on the temperature, local pressure, surface energy, and void radius. The void will grow (i.e., it represents a supercritical nucleus) when the concentration of vacancies in the core $n_v > n_{\text{eq}}$, which provides vacancy fluxes toward the void. Thus, the void nucleation condition vs external pressure p_e , temperature Θ , and radii of the vacancy r_v , core material R_c , and reaction product shell R_s is determined. It is found that the core is under significant compressive pressure due to surface tension, which, according to general wisdom, should suppress void nucleation and growth. However, a nontrivial point of our results is that *compressive pressure promotes void nucleation* by essentially decreasing n_{eq} at the void surface. Thus, with mechanics, a cluster consisting of $q = 4$ vacancies represents a supercritical nucleus. Similarly, a *temperature decrease promotes nucleation*. However, both a pressure increase and a temperature decrease suppress void growth by reducing the diffusion coefficients. Our model described well the experimental results⁵ for oxidation of Cu NPs of four sizes at three temperatures. The parametric study determined the conditions for promoting void formation in particles of different sizes by controlling pressure, temperature, and internal stresses.

GOVERNING EQUATIONS

Since we apply our model to metal oxidation, we will henceforth call the core a metal and the shell an oxide. While often multiple voids nucleate near the core/shell interface,^{8,25} we placed the void at the center, similar to all previous works. Three different stages will be considered: (1) before void nucleation, (2) with all three regions, and (3) after the metal core has disappeared (Figure 1). According to experiments,⁵ it is assumed that oxide and oxygen do not diffuse into the metal and that $R_c = \text{constant}$. Also, oxidation reaction $xM + 0.5yO_2 \rightarrow M_xO_y$ occurs at the external surface only. Below, subscripts $i = 1$ and $i = 2$ refer to metallic atoms in the core and shell, respectively, subscript s means symmetrization of a tensor, a center dot and colon mean contraction and double contraction of tensors or vectors, which are designated by boldface letters, ∇ and ∇^2 are the gradient and Laplacian operators, and \mathbf{I} is the unit second-rank tensor.

Two diffusion equations are needed to model the diffusion of atoms in the shell and core. Furthermore, the void and outer surface of the NPs grow due to the vacancy annihilation and chemical reaction, respectively. The growth velocities of these surfaces are obtained by the conservation of mass. In this section, the coupled mechanical and diffusion equations as well as equations for growth velocities are derived. While there is a significant change in shape due to mass transport, strains are considered to be *small*, which is confirmed by calculations. For simplicity, the temperature is assumed to be constant during the modeling. Due to the smallness of the strains, there is no need to

distinguish between undeformed (reference) and deformed (actual) volumes. The interstitial and substitutional diffusion equations can be found, e.g., in refs 26–28. We added explicit pressure dependency of the diffusion coefficients and actual vacancy concentration dependence of the self-diffusion coefficient to the classic equations.

Diffusion in the Core. The description of self-diffusion of atoms in a core requires consideration of two components, vacancy and metallic atoms.

Flux. In the framework of linear thermodynamics, one can derive the proportionality relation between the diffusive flux \mathbf{j} and its conjugate driving force, the gradient of the chemical potential:^{29–31}

$$\mathbf{j}_1 = -c_1 b_1 \nabla \bar{\mu},$$

$$\bar{\mu} = \mu_1 - \mu_v = \left. \frac{\partial \psi}{\partial c_1} \right|_{\epsilon, \Theta} - \left. \frac{\partial \psi}{\partial c_v} \right|_{\epsilon, \Theta} \quad (1)$$

where μ_1 and μ_v are the chemical potentials of metallic atoms and vacancies, ψ is the free energy per unit volume, c_1 and c_v are the molar concentrations (i.e., number of moles per unit volume) of metallic atoms and vacancies, and b_1 is the atomic mobility. The derivatives in eq 1 are evaluated at fixed strain tensor ϵ and temperature Θ . While it is convenient to perform some derivations using c_1 and c_v , the final results are more tractable in terms of n_1 and n_v , the molar fractions (i.e., number of moles of a specie per total number of moles) of the metallic atoms and vacancies in the core. They are related by $n_1 = c_1/c$, $n_v = c_v/c$, $c = c_1 + c_v$, and $n_v = 1 - n_1$.²⁹ By definition, the molar volume of a metal with vacancies is $\bar{V} = 1/c$.²⁹ Due to the small concentration of vacancies and corresponding small change in volume due to vacancies, the molar volume of metal $\bar{V}_m \simeq \bar{V}$; due to small elastic and thermal strains, we assume that these molar volumes are constant. Thus, $n_1 = \bar{V}_m c_1$ and $n_v = \bar{V}_m c_v$. Therefore, eq 1 can be rewritten as

$$\mathbf{j}_1 = -\frac{n_1 b_1}{\bar{V}_m} \nabla \bar{\mu} = \mathbf{J}_1 / \bar{V}_m, \quad \mathbf{J}_1 = n_1 b_1 \nabla \bar{\mu} \quad (2)$$

in terms of the flux \mathbf{J}_1 and the molar fraction. Such a definition of the flux can be found, for example, in ref 26. The free energy per unit volume for a stressed ideal solution is³²

$$\psi(c_1, \Theta, \epsilon) = \psi^{\text{mech}}(\epsilon) + \psi^{\text{d}}(c_1, \Theta)$$

$$\psi^{\text{d}}(c_1, \Theta) = c_1 \mu_1^\circ + c_v \mu_v^\circ$$

$$+ R\Theta \left[c_1 \ln \frac{c_1}{c_1 + c_v} + c_v \ln \frac{c_v}{c_1 + c_v} \right]$$

$$\psi^{\text{mech}} = 0.5 \epsilon_e : \mathbf{E} : \epsilon_e \quad (3)$$

where R is the gas constant, μ_1° and μ_v° are the standard chemical potentials of metallic atoms and vacancies, \mathbf{E} is the elastic modulus tensor, ψ^{d} and ψ^{mech} are the free energies of an ideal solution and strain energy per unit volume, and ϵ_e is the elastic strain tensor. The total strain tensor is decomposed to the diffusional ϵ_d , thermal ϵ_Θ , and elastic ϵ_e parts:

$$\epsilon = \epsilon_e + \epsilon_d + \epsilon_\Theta, \quad \epsilon_d = \omega'_v (c_v - c_v^{\text{eq}}) \mathbf{I} / 3,$$

$$\epsilon_\Theta = \alpha_1 (\Delta \Theta) \mathbf{I} \quad (4)$$

where α_1 is the linear thermal expansion coefficient of a core, $\Delta \Theta = \Theta - \Theta_r$ ($\Theta_r = 300$ K is the room temperature), ω'_v is the

volumetric diffusion expansion coefficient of vacancies in the metal, and c_{v0}^{eq} is the equilibrium molar concentration of vacancies at the initial pressure and simulation temperature. According to the definition of the chemical potential eq 1

$$\bar{\mu} = \frac{\partial\psi}{\partial c_1} \Big|_{\epsilon} - \frac{\partial\psi}{\partial c_v} \Big|_{\epsilon} = \left[\frac{\partial\psi^d}{\partial c_1} + \frac{\partial\psi^{mech}}{\partial c_1} \Big|_{\epsilon} \right] - \left[\frac{\partial\psi^d}{\partial c_v} + \frac{\partial\psi^{mech}}{\partial c_v} \Big|_{\epsilon} \right] \quad (5)$$

After substitution of eq 3 into eq 5, the chemical potential can be written as

$$\bar{\mu} = \left[\frac{\partial\psi^d}{\partial c_1} \right] - \left[\frac{\partial\psi^d}{\partial c_v} + \frac{\partial\psi^{mech}}{\partial \epsilon_e} \Big|_{\epsilon} : \frac{\partial \epsilon_e}{\partial \epsilon_d} : \frac{\partial \epsilon_d}{\partial c_v} \right] = \mu_1^{\circ} - \mu_v^{\circ} + R\Theta \ln \frac{n_1}{n_v} - \omega'_v p \quad (6)$$

We took into account that $\sigma = \partial\psi^{mech}/\partial\epsilon_e$ is the stress tensor, $\partial\epsilon_e/\partial\epsilon_d$ is the negative fourth-rank unit tensor, $(\partial\psi^{mech}/\partial\epsilon_e)|_{\epsilon} : (\partial\epsilon_e/\partial\epsilon_d) : (\partial\epsilon_d/\partial c_v) = -\sigma : \mathbf{I} \omega'_v / 3 = p \omega'_v$, where $p = -\sigma : \mathbf{I} / 3$ is the pressure.

The diffusional strain can be rewritten as $\epsilon_d = \omega_v(1 - n_1 - n_v^{eq})\mathbf{I}/3$ with the volumetric expansion coefficient $\omega_v = \omega'_v/\bar{V}_m$, $n_v = \bar{V}_m c_v = (1 - n_1)$, and n_v^{eq} for the equilibrium molar fraction of vacancies at the initial pressure and simulation temperature. Then the chemical potential is²⁶

$$\mu = \mu_1^{\circ} - \mu_v^{\circ} + R\Theta \ln \frac{n_1}{1 - n_1} - \bar{V}_m \omega_v p \quad (7)$$

Substituting eq 7 into eq 2, we obtain

$$\mathbf{J}_1 = -b_1 n_1 \nabla \bar{\mu} = -b_1 n_1 \left[\frac{R\Theta \nabla n_1}{n_1 n_v} - \omega_v \bar{V}_m \nabla p \right] \quad (8)$$

Next we elaborate on the equation for the atomic mobility for the substitutional diffusion in the nonequilibrium state:

$$b_1(\Theta, p, n_v) = \frac{D_1}{R\Theta} = \frac{D_v n_v}{R\Theta} = \frac{1}{R\Theta} \frac{D_1^{eq} n_v}{n_{eq}} \quad (9)$$

Here $D_1^{eq} = D_1^0 \exp(-(E_1^a + p\Delta V_1/R\Theta)) = D_{v,eq}$ is the self-diffusion coefficient at the equilibrium concentration of vacancies n_{eq} (D_1^0 , E_1^a , and ΔV_1 are the pre-exponential factor, activation energy, and activation volume of diffusion in the core, respectively) and D_v is the diffusion coefficient of the vacancies. Therefore, the mobility depends on the pressure, temperature, and vacancy concentration. After substitution of eq 9 into eq 8, the flux is rewritten as

$$\mathbf{J}_1 = \frac{D_1^{eq}}{n_{eq}} \left[-\nabla n_1 + \frac{n_1(1 - n_1)\omega_v \bar{V}_m \nabla p}{R\Theta} \right] \quad (10)$$

Equilibrium Concentration of Vacancies. The equilibrium concentration of vacancies is³³

$$n_{eq} = \exp\left(-\frac{G_v^f}{R\Theta}\right) = \exp\left(-\frac{H_v^f - \Theta S_v^f}{R\Theta}\right) \quad (11)$$

where H_v^f , S_v^f , and G_v^f are the enthalpy, entropy, and Gibbs energy of vacancy formation. At the interface with a curvature $1/r$, the

Gibbs energy is changed by

$$\Delta G^{cur} = \frac{2\gamma V_f}{r} \quad (12)$$

where γ is the surface energy and $V_f = (1 - f)\Omega_1$ is the formation volume of a vacancy (Ω_1 is the atomic volume of the metal and f is the vacancy relaxation factor). Taking into account eq 12 and $H_v^f = E_v^f + pV_f$, where E_v^f is the formation energy of a vacancy, the equilibrium concentration of vacancies can be written as

$$n_{eq} = \exp\left(-\frac{E_v^f - \Theta S_v^f}{R\Theta}\right) \exp\left(-\frac{pV_f}{R\Theta}\right) \exp\left(\frac{2\gamma V_f}{rR\Theta}\right) \quad (13)$$

For the bulk, the effect of the surface energy (curvature) and the last exponent in eq 13 disappear:

$$n_{eq} = \exp\left(-\frac{E_v^f - \Theta S_v^f}{R\Theta}\right) \exp\left(-\frac{pV_f}{R\Theta}\right) \quad (14)$$

Mass Balance. The mass balance equation for diffusing species is $\dot{n}_1 + \bar{V} \nabla \cdot \mathbf{j}_1 = 0$,^{32,34} and with $\bar{V} \approx \bar{V}_m$ and eq 2, we obtain²⁶

$$\dot{n}_1 + \nabla \cdot \mathbf{J}_1 = 0 \quad (15)$$

Substituting eq 10 into eq 15, the diffusion equation is obtained:

$$\begin{aligned} \dot{n}_1 = & \nabla \cdot \left(\frac{D_1^{eq}}{n_{eq}} \right) \nabla n_1 \\ & + \frac{D_1^{eq}}{n_{eq}} \nabla^2 n_1 - \frac{(1 - n_1)n_1 \omega_v \bar{V}_m \nabla}{R\Theta} \cdot \left(\frac{D_1^{eq}}{n_{eq}} \right) \nabla p \\ & - \frac{D_1^{eq}(1 - 2n_1)\omega_v \bar{V}_m \nabla n_1 \nabla p}{n_{eq} R\Theta} - \frac{D_1^{eq} n_1 (1 - n_1) \omega_v \bar{V}_m \nabla^2 p}{n_{eq} R\Theta} \end{aligned} \quad (16)$$

Since $\nabla(D_1^{eq}/n_{eq}) = -(D_1^{eq}\Delta\bar{V}/R\Theta n_{eq})\nabla p$, with $\Delta\bar{V} = \Delta\bar{V}_1 - V_f$, the diffusion equation can be rewritten as

$$\begin{aligned} \dot{n}_1 = & \frac{D_1^{eq}}{n_{eq}} \left[\nabla^2 n_1 + \frac{(1 - n_1)n_1 \omega_v \bar{V}_m \Delta\bar{V}(\nabla p)^2}{(R\Theta)^2} \right. \\ & \left. - \frac{[(1 - 2n_1)\omega_v \bar{V}_m + \Delta\bar{V}]\nabla n_1 \nabla p}{R\Theta} - \frac{n_1(1 - n_1)\bar{V}_m \omega_v \nabla^2 p}{R\Theta} \right] \end{aligned} \quad (17)$$

Diffusion in the Shell. In the shell, the metallic atoms are diffusing species and oxide atoms act as a matrix. For interstitial diffusion, the flux is defined in the same way as in eq 2:

$$\mathbf{J}_2 = -n_2 b_2 \nabla \mu_2, \quad \mu_2 = \frac{\partial\psi}{\partial c_2} \Big|_{\epsilon, \Theta} \quad (18)$$

where the subscript 2 is for metal atoms in the shell. The atomic mobility is

$$b_2(\Theta, p) = \frac{D_2}{R\Theta}, \quad D_2 = D_2^0 \exp\left(-\frac{E_2^a + p\Delta V_2}{R\Theta}\right) \quad (19)$$

The free energy per unit volume for a stressed ideal solution is similar to eq 3:

$$\begin{aligned} \psi(c_2, \Theta, \boldsymbol{\varepsilon}) &= \psi^{\text{mech}}(\boldsymbol{\varepsilon}) + \psi^{\text{d}}(c_2, \Theta) \\ \psi^{\text{d}}(c_2, \Theta) &= c_2 \mu_2^{\circ} + c_h \mu_h^{\circ} \\ &+ R\Theta \left[c_2 \ln \frac{c_2}{c_2 + c_h} + c_h \ln \frac{c_h}{c_2 + c_h} \right] \\ \psi^{\text{mech}} &= 0.5 \boldsymbol{\varepsilon}_e : \boldsymbol{\varepsilon}_e \end{aligned} \quad (20)$$

where μ_2° and μ_h° are standard chemical potentials of diffusing and matrix atoms and c_2 and c_h are the molar concentrations of diffusing and matrix atoms. The chemical potential can be calculated similarly to the substitutional diffusion:^{26,28}

$$\mu_2 = \mu_2^{\circ} + R\Theta \ln n_2 + \omega_2 \bar{V}_s p \quad (21)$$

where \bar{V}_s is the molar volume of a matrix (oxide).

Flux. Combining eqs 18, 19, and 21, the flux of diffusing atoms in the shell can be expressed as

$$\mathbf{J}_2 = -D_2 \left[\nabla n_2 + \frac{n_2 \omega_2 \bar{V}_s \nabla p}{R\Theta} \right] \quad (22)$$

Mass Balance. The mass balance equation for metal atoms in the shell is

$$\dot{n}_2 + \nabla \cdot \mathbf{J}_2 = 0 \quad (23)$$

Substituting eq 22 into eq 23, we obtain the diffusion equation:

$$\begin{aligned} \dot{n}_2 &= D_2 \left[\nabla^2 n_2 + \frac{1}{R\Theta} (\omega_2 \bar{V}_s - \Delta V_2) \nabla n_2 \nabla p \right. \\ &\left. + \frac{\omega_2 \bar{V}_s n_2 \nabla^2 p}{R\Theta} - \frac{\omega_2 \Delta V_2 \bar{V}_s n_2 (\nabla p)^2}{(R\Theta)^2} \right] \end{aligned} \quad (24)$$

Mass Balance for the Outer Surface. When the metal atoms reach the outer surface and react with the oxygen, it is assumed that the reaction rate is infinite; i.e., all metallic atoms that reach the outer surface react with oxygen instantaneously and form the oxide layer on the outer surface. If metallic atoms will deposit on the external surface without reaction, then the outer boundary normal velocity $v = \mathbf{J}_2 \cdot \mathbf{n}$, where \mathbf{n} is the unit outer normal to the interface. For a general oxidation reaction, $xM + 0.5yO_2 \rightarrow M_xO_y$, instead of the volume of x moles of metal, $x\bar{V}_m$ one obtains the volume of 1 mol of oxide, \bar{V}_s . Thus

$$v = \frac{\bar{V}_s \mathbf{J}_2 \cdot \mathbf{n}}{x\bar{V}_m} \quad (25)$$

Mass Balance for the Void Interface. The velocity of the void interface is

$$\dot{a} = (\mathbf{J}_v^+ - \mathbf{J}_v^-) \cdot \mathbf{n} / (n_v^+ - n_v^-) \quad (26)$$

where superscript “−” denotes a core and “+” indicates a void. The vacancy concentration in the void region $n_v^+ = 1$ and near the void surface $n_v^- = n_{\text{eq}}$ according to boundary conditions; additionally, $\mathbf{J}_v^+ = 0$. In the core, the metallic atoms exchange their positions with vacancies. Therefore, the flux of vacancies is equal to the negative flux of metallic atoms:

$$\mathbf{J}_v^- = -\mathbf{J}_1 = -\frac{D_1^{\text{eq}}}{n_{\text{eq}}} \left[-\nabla n_1 + \frac{(1-n_1)n_1\omega_v\bar{V}_m\nabla p}{R\Theta} \right] \quad (27)$$

Also, the unit normal vector on the void surface is negative. Substituting eq 27 into eq 26, one obtains the velocity of the void growth:

$$\dot{a} = -\frac{D_1^{\text{eq}}}{n_{\text{eq}}(1-n_{\text{eq}})} \left[-\nabla n_1 + \frac{(1-n_1)n_1\omega_v\bar{V}_m\nabla p}{R\Theta} \right] \quad (28)$$

COMPLETE COUPLED SYSTEM OF EQUATIONS

Below we will collect only those equations that are used in numerical simulations for spherically symmetric problem formulation.

(1) Diffusion of metallic atoms in the core:

$$\begin{aligned} \dot{n}_1 &= \frac{D_1^{\text{eq}}}{n_{\text{eq}}} \left[\nabla^2 n_1 + \frac{(1-n_1)n_1\omega_v\bar{V}_m\Delta\bar{V}(\nabla p)^2}{(R\Theta)^2} \right. \\ &\left. - \frac{[(1-2n_1)\omega\bar{V}_m + \Delta\bar{V}]\nabla n_1\nabla p}{R\Theta} \right. \\ &\left. - \frac{n_1(1-n_1)\bar{V}_m\omega_v\nabla^2 p}{R\Theta} \right] \end{aligned} \quad (29)$$

(2) Diffusion of metallic atoms in the shell:

$$\begin{aligned} \dot{n}_2 &= D_2 \left[\nabla^2 n_2 + \frac{1}{R\Theta} (\omega_2 \bar{V}_s - \Delta V_2) \nabla n_2 \nabla p \right. \\ &\left. + \frac{\omega_2 \bar{V}_s n_2 \nabla^2 p}{R\Theta} - \frac{\omega_2 \Delta V_2 \bar{V}_s n_2 (\nabla p)^2}{(R\Theta)^2} \right], \\ D_i &= D_i^0 \exp\left(-\frac{E_i^a + \Delta V_i p}{R\Theta}\right), \quad i = 1, 2 \end{aligned} \quad (30)$$

(3) Equilibrium concentration of vacancies in the bulk:

$$n_{\text{eq}} = \exp\left(-\frac{E_v^f - \Theta S_v^f}{R\Theta}\right) \exp\left(-\frac{pV_f}{R\Theta}\right) \quad (31)$$

(4) Strain–displacement relationship and strain decomposition:

$$\begin{aligned} \boldsymbol{\varepsilon} &= (\nabla \mathbf{u})_s, \quad \boldsymbol{\varepsilon} = \boldsymbol{\varepsilon}_e + \boldsymbol{\varepsilon}_\Theta + \boldsymbol{\varepsilon}_d, \\ \boldsymbol{\varepsilon}_\Theta &= \alpha_i(\Delta\Theta)\mathbf{I}, \quad \boldsymbol{\varepsilon}_d^1 = \omega_v(1-n_1-n_{v0}^{\text{eq}})\mathbf{I}/3, \\ \boldsymbol{\varepsilon}_d^2 &= \omega_2 n_2 \mathbf{I}/3 \end{aligned} \quad (32)$$

(5) Hooke's law, pressure, and equilibrium equation:

$$\boldsymbol{\sigma} = \mathbf{E}:\boldsymbol{\varepsilon}_e, \quad p = -\boldsymbol{\sigma}:\mathbf{I}/3, \quad \nabla \cdot \boldsymbol{\sigma} = 0 \quad (33)$$

The coupled system of eqs 29–33 is solved numerically for the three different stages in our problem: (1) before void nucleation, (2) with all three regions, and (3) after the metal core has disappeared (Figure 1). The following boundary conditions are applied in each stage.

(1) Before void nucleation:

$$\begin{aligned} \text{at } r = 0: \quad & J_1 = 0, \quad u = 0 \\ \text{at } r = R_c = \text{constant}: \quad & u_1 = u_2, \\ & \sigma_r^1 - \sigma_r^2 = -2\gamma_{cs}/R_c, \quad J_1 = J_2, \quad n_2 \leq n_{\max} \\ \text{at } r = R_s: \quad & \sigma_r^2 = -2\gamma_s/R_s + p_e, \quad n_2 = 0, \\ & \dot{R}_s = -J_2\bar{V}_s/x\bar{V}_m \end{aligned} \quad (34)$$

(2) With all three regions:

$$\begin{aligned} \text{at } r = a: \quad & 1 - n_1 = n_v = n_{\text{eq}} \\ & = \exp\left(-\frac{E_v^f - \Theta S_v^f}{R\Theta}\right) \exp\left(-\frac{p(a)V_f}{R\Theta}\right) \exp\left(\frac{2\gamma V_f}{rR\Theta}\right), \\ & \sigma_r = -2\gamma_a/a, \quad \dot{a} = -J_1/(1 - n_{\text{eq}}) \\ \text{at } r = R_c = \text{constant}: \quad & u_1 = u_2, \\ & \sigma_r^1 - \sigma_r^2 = -2\gamma_{cs}/R_c, \quad J_1 = J_2, \\ & n_2 \leq n_{\max} \\ \text{at } r = R_s: \quad & \sigma_r^2 = -2\gamma_s/R_s + p_e, \quad n_2 = 0, \\ & \dot{R}_s = -J_2\bar{V}_s/x\bar{V}_m \end{aligned} \quad (35)$$

(3) After the metal core has disappeared:

$$\begin{aligned} \text{at } r = R_c = \text{constant}: \quad & J_1 = 0, \quad \sigma_r = -2\gamma_a/a \\ \text{at } r = R_s: \quad & \sigma_r^2 = -2\gamma_s/R_s + p_e, \quad n_2 = 0, \\ & \dot{R}_s = -J_2\bar{V}_s/x\bar{V}_m \end{aligned} \quad (36)$$

For all cases, the fluxes are

$$\begin{aligned} J_1 &= \frac{D_1^{\text{eq}}}{n_{\text{eq}}} \left[-\nabla n_1 + \frac{(1 - n_1)n_1\omega_v\bar{V}_m}{R\Theta} \nabla p \right], \\ J_2 &= -D_2 \left[\nabla n_2 + \frac{n_2\omega_2\bar{V}_s}{R\Theta} \nabla p \right] \end{aligned} \quad (37)$$

n_{\max} is the maximum solubility of metal in the oxide. Equations 34–36 contain continuity of displacements and fluxes of metal atoms, as well as jump conditions for radial stresses σ_r . The condition $n_2 = 0$ at $r = R_s$ is the consequence of the assumption of an infinite reaction rate. Indeed, as soon as metal atoms appear at the external surface, they are consumed by reaction. The condition in eq 35 for the vacancy concentration n_v means that at the void surface it is always equal to n_{eq} , similar to the results in ref 15. In addition to the dependence of n_{eq} on the temperature and surface, we took into account the effect of the pressure p , which, as was shown, is very important.

Initial Conditions. As an initial state, we consider a core/shell system without a void at a chosen temperature Θ , which produces initial stresses $\boldsymbol{\sigma}^{\text{in}}$ (in particular, pressure p^{in}) due to different thermal expansion coefficients of the core and shell. In addition

$$\begin{aligned} \text{core:} \quad & 1 - n_1 = n_v = n_{v0}^{\text{eq}} = e^{-(E_v^f - S_v^f\Theta)/R\Theta} e^{-V_f p^{\text{in}}/R\Theta} \\ \text{shell:} \quad & n_2 = 0 \end{aligned} \quad (38)$$

Note that p_1^{in} can be calculated analytically using eq 40. For example, $p_1^{\text{in}} = 0.716$ GPa for $R_c = 9.05$ nm at 373 K. The solution from the previous stage is used as the initial condition for the next stage.

MATERIAL PARAMETERS

We use in the calculations the following material parameters for Cu/Cu₂O nanoparticles: radii of vacancy, $r_v = 0.199$ nm; atomic volume of Cu, $\Omega_1 = 1.18 \times 10^{-29}$ m³/atom, and vacancy relaxation factor, $f = 0.3$, i.e., $V_f = 0.7\Omega_1$ m³/atom;³⁵ Cu elastic shear, $G_1 = 22.5$ GPa, and bulk, $K_1 = 143.33$ GPa, moduli;³⁶ Cu₂O elastic shear, $G_2 = 8$ GPa, and bulk, $K_2 = 111.33$ GPa, moduli;³⁷ Cu linear thermal expansion coefficient, $\alpha_1 = 1.72 \times 10^{-5}$ °C⁻¹;³⁸ Cu₂O linear thermal expansion coefficient, $\alpha_2 = 1.05 \times 10^{-6}$ °C⁻¹;³⁹ Cu molar volume, $\bar{V}_m = 7.1 \times 10^{-6}$ m³/mol; Cu₂O molar volume, $\bar{V}_s = 23.31 \times 10^{-6}$ m³/mol;⁵ volumetric diffusion expansion coefficient of vacancies in Cu, $\omega_v = -0.3$;³⁵ volumetric diffusion expansion coefficient of Cu in Cu₂O, $\omega_2 = 0.256$;⁴⁰ pre-exponential factor for the self-diffusion coefficient of Cu, $D_1^0 = 7.8 \times 10^{-5}$ m²/s; activation energy for Cu self-diffusion coefficient, $E_1^a = 211.3$ kJ/mol;⁴¹ surface energy of Cu, $\gamma_a = 1.79$ J/m²;⁴² (due to the lack of experimental data, we assumed that the surface energies of the core/shell interface, γ_{cs} , and Cu₂O surface, γ_s , are equal to the Cu surface energy, γ_a); activation volume of the self-diffusion coefficient, $\Delta V_1 = 0.6\Omega_1$ m³/atom³⁰ (due to lack of data, we assumed that $\Delta V_2 = \Delta V_1$); energy of vacancy formation of Cu; $E_v^f = 103.24$ kJ/mol; entropy of vacancy formation of Cu, $S_v^f = 1.46 \times 10^{-5}$ R.⁴³

The diffusion coefficient of Cu in Cu₂O at the nanoscale, D_2 , and maximum solubility of Cu in Cu₂O could not be found in the literature. At the macroscale, D_2 is on the order of 10^{-24} m²/s⁴⁴ at $\Theta = 373$ K; however, it is expected to be much larger at the nanoscale. To justify this, we analyze available data for diffusion of Al in aluminum oxide. Thus, for bulk material the diffusion coefficient of Al in α -alumina at 800–950 °C is $D = 10^{-18}$ cm²/s.⁴⁵ Data collected in ref 7 show the same order of magnitude but for 1200 °C. In molecular dynamics simulations, the diffusivity of aluminum⁴⁶ has an extremely high order of magnitude of 10^{-4} cm²/s at 400 K. In ref 47, the diffusion coefficient of Al in various types of alumina (amorphous and crystalline) has been determined for particle radii from 2.8 to 4 nm and oxide shells from 1 to 2 nm using molecular dynamics. For 1000 K, the value of $D_4 \approx 10^{-5}$ cm²/s has been obtained. In ref 48, $D \approx 4 \times 10^{-9}$ cm²/s at 873 K was obtained to fit the oxidation time of a nanoparticle to the experimental value of 1 s. Independent of significant scatter, the drastic increase in the diffusion coefficient for the nanoscale particles and shell is clearly visible.

Thus, these parameters, D_2 and n_{\max} will be found by fitting experiments. First, we found $D_2(373 \text{ K}) = 10^{-18}$ m²/s and $n_{\max} = 0.009$, which give good consistency with the experimental data on the oxide thickness $\delta = R_s - R_c$ vs time t for a particle with $R_c = 9.05$ nm at $\Theta = 373$ K. Second, keeping n_{\max} , the diffusion coefficient D_2 of Cu in Cu₂O was varied to fit the experimental

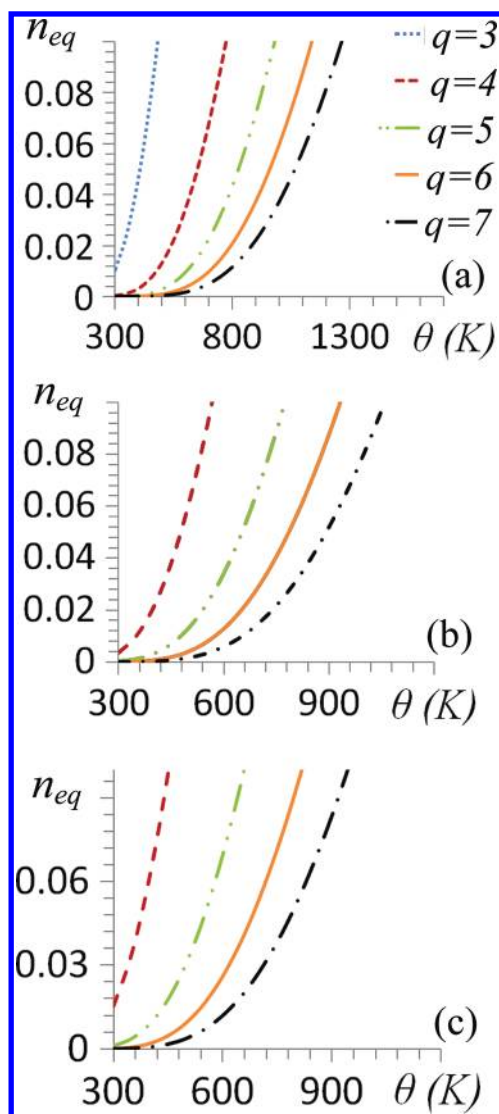


Figure 2. Equilibrium concentration of vacancies (eq 35) at the surface of a void consisting of q vacancies vs temperature for different external pressures at the void surface: (a) $p(a) = 2$ GPa, (b) $p(a) = 0.716$ GPa, and (c) $p(a) = 0$.

data for a particle with $R_c = 4.26$ nm at $\Theta = 323$ K. With these two fitted diffusion coefficients, one can extract $D_1^0 = 4.017 \times 10^{-12}$ m^2/s and $E_2^a = 47.156$ kJ/mol.

VOID NUCLEATION CRITERION

At the moving void surface of radius a , we assumed that the vacancy concentration n_v is always equal to its equilibrium value n_{eq} , similar to the results of ref 15. In addition to the dependence of n_{eq} on the temperature Θ and surface energy γ in ref 15, we took into account the effect of pressure $p(a)$ at the void surface (eq 35), which, as will be shown below, is very important. We will define the supercritical void as the void that can grow, i.e., when n_{eq} at its surface is smaller than n in the surroundings. Then vacancy flux will be directed toward the void and cause its growth. The radius of the void, which represents the q -vacancy cluster, is determined by $a = r_v q^{1/3}$. This approximation shows good correspondence with the data in ref 35 for stable three- and four-vacancy clusters in Cu. Plots of the equilibrium concentration of

vacancy n_{eq} (eq 35) at the surface of the void consisting of q vacancies vs temperature for several values of q and pressure are shown in Figure 2. The smaller value n_{eq} has the larger probability of void nucleation, because it is easier to reach and exceed this value in the surroundings of a void. The main *counterintuitive conclusion* coming from Figure 2 is that compressive pressure promotes supercritical void nucleation. Indeed, general wisdom is that pressure suppresses void formation. However, in our case, pressure, reducing n_{eq} at the void surface, promotes transport of vacancies toward the void, causing void growth. Note that the promoting effect of pressure on void nucleation, based on a completely different consideration, was found in ref 49. It follows from eq 35 that at $\Theta = 323$ K and $p = 0.716$ GPa (which corresponds, e.g., to a free particle with $R_c = 9.05$ nm and $R_s = 11.55$ nm), allowing for pressure reduces n_{eq} by a factor of 3.8. Also, temperature suppresses supercritical void nucleation.

Below, we connect the external pressure p_e and pressure at the void surface, assuming homogeneous distribution of n_1 and n_2 . First, an elastic solution for a hollow sphere⁵⁰ results in the following pressure distribution in the core:

$$p(r) = \frac{(-2\gamma_1 W^3/a - \sigma_r^1(R_c))/(1 - W^3)}{W = a/R_c} \quad (39)$$

where σ_r^1 is the radial stresses in the core. For nucleation $W \ll 1$ and one obtains $p(a) = -\sigma_r^1(R_c)$, which is independent of the surface tension at the void surface. Thus, a very small void, while changing all stresses, does not change the pressure in a core and keeps the pressure in a core homogeneous. To connect the external pressure p_e with pressure in a core, we can use the equation for a solid core/shell system:³

$$p = \frac{12(m^3 - 1)(\Delta\epsilon^{in})G_2K_1K_2}{H} + \frac{2K_1(4G_2 + 3m^3K_2)\gamma_1}{R_sH} + \frac{(2\gamma_2 + p_e R_s m)m^2K_1(4G_2 + 3K_2)}{R_sH} \quad (40)$$

where $m = R_s/R_c$

$$\Delta\epsilon^{in} = (\alpha_2 - \alpha_1)\Delta\Theta + \frac{1}{3}[\omega_2 n_2 - \omega_1(n_v - n_{eq})],$$

$$H = 3K_1K_2m^3 + 4G_2(K_1 + (m^3 - 1)K_2)$$

(41)

K_i and G_i are the bulk and shear elastic constants. Equation 40 allows one to predict the effect of various particle parameters, external pressure, and temperature on the pressure in the core for small void size (in particular, during nucleation) and, consequently, on the nucleation condition. Thus, external pressure essentially increases p , but this increase reduces with m . n_1 and n_2 decrease p , and this decrease grows with m . Also, a temperature rise slightly increases pressure, and this rise grows with m . An increase in particle size reduces the pressure contribution due to surface tension, which is the only pressure source for $p_e = 0$.

NUMERICAL METHOD

The finite element method code COMSOL Multiphysics was utilized to iteratively solve the coupled system of eqs 29–33 for each time step. Displacement and concentration fields have been considered as primary variables. Solutions of the equations of elasticity theory for given n_1 and n_2 distributions have been obtained using the Structural Mechanics module of COMSOL at

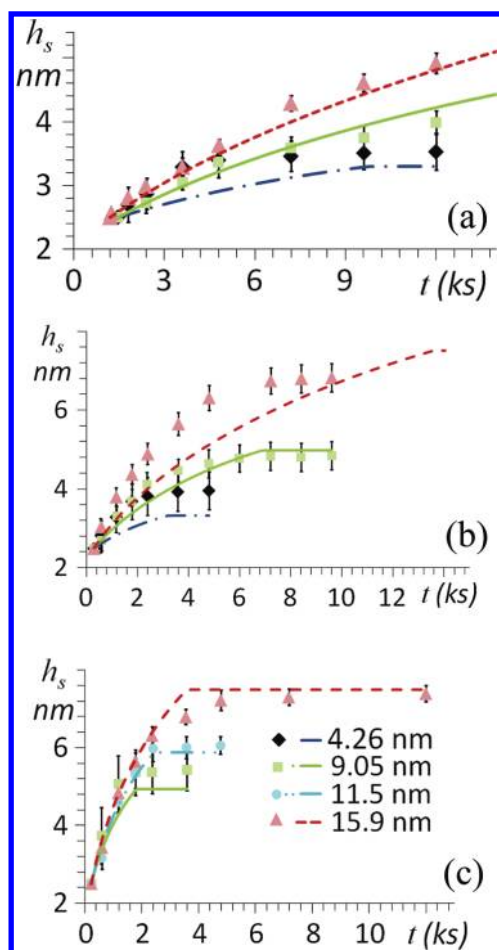


Figure 3. Oxide layer thickness vs time for Cu NPs of four different core radii: lines are results of simulations, and symbols are results of experiments from ref 5. Key: (a) $\Theta = 323$ K, (b) $\Theta = 343$ K, and (c) $\Theta = 373$ K.

each time step. After nodal displacements are found, strains and stresses (including pressure) can be found using eqs 32 and 33. The pressure field was used for solutions of diffusion eqs 29–31 for the same time step in the main module of COMSOL Multiphysics. After increments of a and R_s were obtained by integrating eq 35, the geometry was updated using the Arbitrary Lagrangian–Eulerian (ALE) technique. Quintic Lagrangian elements are used for both the mechanical and diffusion equations. The total number of integration points was 1290, and the time step varied from 0.001 to 0.15 s in different stages.

Note that all of the main types of pressure distributions for each of the three stages were compared with the developed analytical solution and that the results are in very good correspondence. Our analytical solution generalizes this in ref 51 for the case with the prescribed heterogeneous n_1 and n_2 distributions, which was taken from numerical simulations.

VOID AND OXIDE GROWTH

Oxide Growth. We simulated the oxidation and hollow formation and growth for three temperatures (323, 343, and 373 K) and four NP core radii (4.26, 9.05, 11.5, and 15.9 nm) with an initial shell thickness of 2.5 nm.⁵ For $R_c = 9.05$ nm at $\Theta = 373$ K, when n_v at the center reaches $n_{eq} = 0.0154$, a four-vacancy

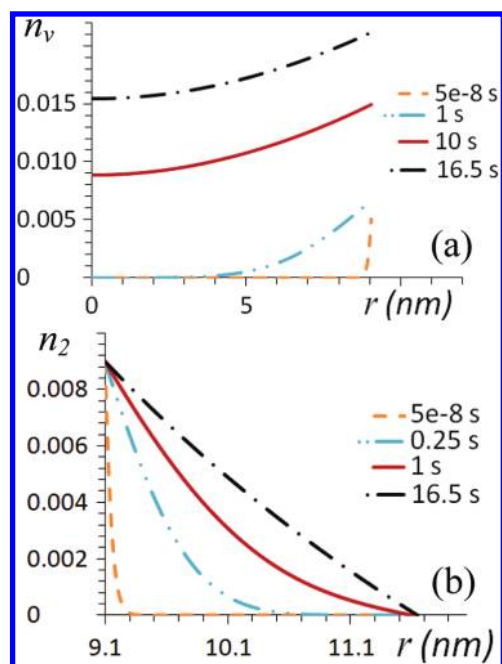


Figure 4. Evolution of the distribution of vacancy concentration in a core (a) and Cu atoms in a shell (b) for $R_c = 9.05$ nm at $\Theta = 373$ K.

nanovoid is introduced at the center of the NP. Comparison of the results of numerical simulation for the oxide layer thickness h_s vs time for Cu particles of four different sizes with experiments in Figure 3 shows very good consistency; one has to keep in mind significant scatter in particle sizes and shell thicknesses in the experiments. Note that the final oxide thickness is determined by the mass balance, which is satisfied in our simulations. Thus, discrepancy with experiment in the final oxide thickness is related to an error of the presentation of experimental results.

Pressure and Vacancy Distribution for a Solid Core/Shell Structure. Distributions of the concentration of vacancies in a solid core and Cu atoms in a shell are presented in Figure 4 for $R_c = 9.05$ nm at $\Theta = 373$ K. Since Cu atoms diffuse to the shell and react with oxygen, vacancies are generated at the core/shell interface and diffuse to the core center. Both distributions increase in time until 16.5 s, and n_v at the center reaches $n_{eq} = 0.0154$, which is determined by eq 35.

The pressure distribution in the core is slightly heterogeneous due to heterogeneous vacancy distribution and reduces from 0.71 to 0.68 GPa during 16.5 s due to increasing n_v . The pressure distribution in the shell is also slightly heterogeneous, and its maximum increases from 0.325 to 0.345 GPa due to increasing n_2 .

Pressure and Vacancy Distribution for the Void Growth Stage. After n_v at the center reaches $n_{eq} = 0.0154$, a four-vacancy nanovoid is introduced at the center of the NP. The results are presented in Figure 5. With increasing time, vacancies are absorbed by the growing void, and the core becomes smaller until all Cu atoms diffuse to the growing shell. Initially, the sharp reduction in n_v causes fast void growth, which decelerates with time (Figure 6). Initial fast growth is caused by the strong reduction in the equilibrium concentration of vacancies at the void surface with increasing void radius and by the small initial void size. The pressure becomes more homogeneous in the core with increasing time and increases from the initial 0.716 to 1.9 GPa at 1 ks. Note that pressure increases with growing a/R_c and

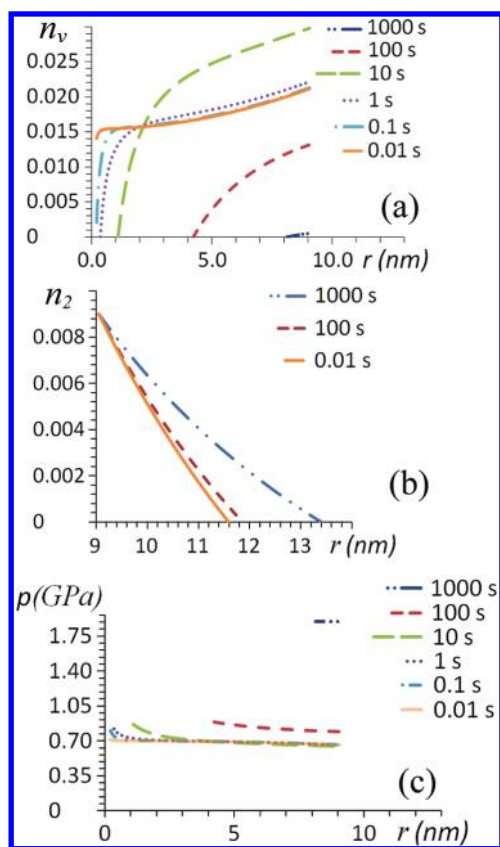


Figure 5. Evolution of the distribution of vacancy concentration in a core (a) and Cu atoms in a shell (b), as well as pressure in a core (c) for $R_c = 9.05$ nm at $\Theta = 373$ K during nanovoid growth.

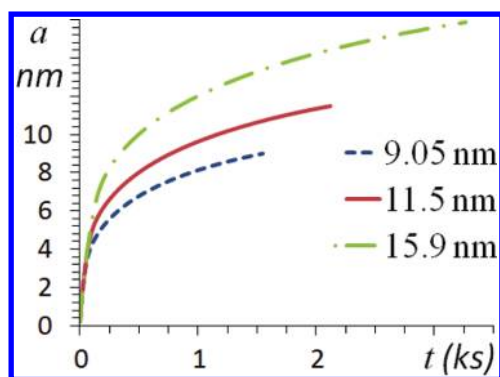


Figure 6. Variation of the void radius vs time for three particle sizes at $\Theta = 373$ K.

decreases with growing R_s/R_c , but the former is larger than the latter. Such a pressure increase decreases the self-diffusion coefficient of Cu by a factor of 5. Also, pressure increases in the shell from the range of 0.324–0.347 GPa to 0.461–0.484 GPa. Note that the pressure gradient term in the diffusion equations promotes diffusion of Cu in the shell, but suppresses diffusion of vacancies. The resultant effect is promoting; when the pressure gradient term is neglected, the time for formation of the maximum-size hole increases by 71 s.

Hollow Oxide. When the metal core disappears, the remnant Cu atoms in a shell diffuse to the outer surface and react with oxygen, until complete disappearance of Cu atoms. This process

takes about 100 s with deceleration in time. Pressure reduces at the void surface from 0.515 to 0.499 GPa, increases at the external surface from 0.495 to 0.499 GPa, and finally becomes homogeneous. The final pressure is caused by surface tension.

COMPARISON WITH EXISTING APPROACHES

There are several main differences between our approach and results and those in refs 17 and 18 which allowed us to obtain good comparison with experiments and to elucidate the void nucleation and growth mechanisms.

- (1) In the general case, one has to include misfit volumetric strain due to chemical reaction, as in refs 17 and 18. In refs 17 and 18, because of misfit strain and neglected compressive stresses due to surface tension, huge tensile stresses in a core (and compressive stresses in a shell) appeared, which led to the idea that they can cause void nucleation due to fracture. However, because in our problem the reaction occurs at the surface (rather than in the bulk) and the interface between the metal and oxide is incoherent, internal stresses due to chemical reaction are negligible. For example, an aluminum oxide shell is amorphous below some thickness (4 nm), and thus, the interface is incoherent and does not generate internal stresses. Even for a crystalline shell, for Al particles with $R_c = 20$ –40 nm and a shell growing during chemical reaction to $m = 1.76$, lattice spacing in Al did not differ from that in the bulk sample;⁵² i.e., internal stresses are negligible. That is why we excluded misfit strain but included surface tension, which resulted in compressive pressure both in the core and shell and in elimination of the fracture hypothesis.
- (2) The suggested void nucleation criterion shows that, surprisingly, compressive pressure promotes void nucleation.
- (3) We took into account that the self-diffusion coefficient is proportional to the actual (rather than equilibrium) concentration of vacancies, which increased it at the initial stage by 12 orders of magnitude. We also took into account that the diffusion coefficient of metal in oxide at the nanoscale is much larger than in bulk material.

CONCLUDING REMARKS

A continuum-mechanochemical approach for nucleation and growth of a nanovoid in reacting NPs is developed that treats explicitly void nucleation and the effects of stresses. A counterintuitive effect of pressure on nucleation is found. Experimental results for Cu NPs are described. On the basis of obtained results, the following regimes can be used to accelerate void formation and make it possible in micrometer-scale particles. Initially, high temperature at zero pressure should be applied to accelerate diffusion and reach the desired level of n_v . Then temperature should be reduced, and pressure may be applied to reduce n_{eq} and cause void nucleation. After the void reaches the size corresponding to low-enough n_{eq} , pressure should be removed and temperature increased to accelerate diffusion. Accordingly, to suppress void nucleation by the above mechanism, one has to increase temperature and tensile pressure, and to suppress void growth, one has to reduce temperature and apply compressive pressure. A similar continuum framework can be used for modeling the nanotube fabrication on the basis of the Kirkendall

effect.⁵³ Note that it is understood that application of continuum methods to such small nuclei can be questioned. However, continuum concepts are successfully applied even to a single vacancy (see ref 54 and the concept of the center of dilatation) and are routinely used in nucleation theory for a critical nucleus consisting of a few atoms (see examples in ref 19).

AUTHOR INFORMATION

Corresponding Author

*Phone: (515) 294-9691. Fax: (801) 788-0026. E-mail: vlevitas@iastate.edu.

Notes

[†]E-mail: hamed82@iastate.edu.

ACKNOWLEDGMENT

The support of the National Science Foundation, Air Force Office of Scientific Research, and Iowa State University is gratefully acknowledged.

REFERENCES

- (1) Hosokawa, M.; Nogi, K.; Naito, M.; Yokoyama, T. *Nanoparticle Technology Handbook*; Elsevier: New York, 2007; p 100.
- (2) Shpak, A. P.; Gorbyk, P. P. *Nanomaterials and Supramolecular Structures: Physics Chemistry, and Applications*; Springer: New York, 2009; p 207.
- (3) Levitas, V. I.; Asay, B. W.; Son, S. F.; Pantoya, M. *J. Appl. Phys.* **2007**, *101*, 083524.
- (4) Yin, Y.; Rioux, R. M.; Erdonmez, C. K.; Hughes, S.; Somorjai, G. A.; Alivisatos, A. P. *Science* **2004**, *304*, 711–714.
- (5) Tokozakura, D.; Nakamura, R.; Nakajima, H.; Lee, J. G.; Mori, H. *J. Mater. Res.* **2007**, *22*, 2930–2935.
- (6) Hung, L. I.; Tsung, C. K.; Huang, W.; Yang, P. *Adv. Mater.* **2010**, *22*, 1910–1914.
- (7) Nakamura, R.; Tokozakura, D.; Nakajima, H.; Lee, J. G.; Mori, H. *J. Appl. Phys.* **2007**, *101*, 074303.
- (8) Wang, C. M.; Baer, D. R.; Thomas, L. E.; Amonette, J. E.; Antony, J.; Qiang, Y.; Duscher, G. *J. Appl. Phys.* **2005**, *98*, 094308.
- (9) Cabot, A.; Pantes, V. F.; Shevchenko, E.; Yin, Y.; Balcells, L.; Marcus, A. M.; Hughes, M.; Alivisatos, A. P. *J. Am. Chem. Soc.* **2007**, *129*, 10358–10360.
- (10) Yin, Y.; Erdonmez, C. K.; Cabot, A.; Hughes, M.; Alivisatos, A. P. *Adv. Funct. Mater.* **2006**, *16*, 1389–1399.
- (11) Cabot, A.; Ibanez, M.; Guardia, P.; Alivisatos, A. P. *J. Am. Chem. Soc.* **2009**, *131*, 11326–11328.
- (12) Smigelskas, A. D.; Kirkendall, E. O. *Trans. Am. Inst. Min., Metall. Eng.* **1947**, *171*, 130–142.
- (13) Evteev, A. V.; Levchenko, E. V.; Belova, I. V.; Murch, G. E. *J. Nano Res.* **2009**, *7*, 11–17.
- (14) Gusak, A. M.; Zaporozhets, T. V. *J. Phys.: Condens. Matter* **2009**, *21*, 415303.
- (15) Yu, H. C.; Yeon, D. H.; Li, X. F.; Thornton, K. *Acta Mater.* **2009**, *57*, 5348–5360.
- (16) Gusak, A. M.; Tu, K. N. *Acta Mater.* **2009**, *57*, 3367–3373.
- (17) Svoboda, J.; Fischer, F. D.; Vollath, D. *Acta Mater.* **2009**, *57*, 1912–1919.
- (18) Zhdanov, V. P.; Kasemo, B. *Nano Lett.* **2009**, *9* (5), 2172–2176.
- (19) Levitas, V. I.; Altukhova, N. *Phys. Rev. Lett.* **2008**, *101* (14), 145703.
- (20) Levitas, V. I.; Altukhova, N. *Phys. Rev. B* **2009**, *79* (21), 212101.
- (21) Levitas, V. I.; Altukhova, N. *Acta Mater.* **2011**, *59* (18), 7051.
- (22) Rokkam, S.; El-Azab, A.; Millett, P.; Wolf, D. *Modell. Simul. Mater. Sci. Eng.* **2009**, *17*, 064002.
- (23) Yu, H. C.; Lu, W. *Acta Mater.* **2005**, *53* (6), 1799–1807.
- (24) Levitas, V. I.; Idesman, A. V.; Palakala, A. *J. Appl. Phys.* **2011**, *110* (3), 033531.
- (25) Railsback, J. G.; Johnston-Peck, A. C.; Wang, J. W.; Tracy, J. B. *ACS Nano* **2010**, *4* (4), 1913–1920.
- (26) Larche, F. C.; Cahn, J. W. *Acta Mater.* **1982**, *30*, 1835–1845.
- (27) Yang, F. *Mater. Sci. Eng., A* **2005**, *409*, 153–159.
- (28) Li, J. C. M. *Metall. Trans. A* **1978**, *9A*, 1353–1380.
- (29) Balluffi, R. W.; Allen, S. M.; Carter, W. C.; Kemper, R. A. *Kinetics of Material*, 2nd ed.; John Wiley: Hoboken, NJ, 2005; p 24.
- (30) Bakker, H.; Mehrer, H. *Diffusion in Solid Metals and Alloys*; Springer: New York, 1990; p 607.
- (31) Svoboda, J.; Fischer, F. D.; Fratzl, P.; Kroupa, A. *Acta Mater.* **2002**, *50*, 1369–1381.
- (32) Larche, F. C.; Chan, J. W. *Acta Mater.* **1985**, *3*, 331–357.
- (33) Porter, D. A.; Eastirling, K. E. *Phase Transformation in Metals and Alloys*, 2nd ed.; Chapman and Hall: London, 1992; p 45.
- (34) Fischer, F. D.; Svoboda, J. *Scr. Mater.* **2007**, *58*, 93–95.
- (35) Nemirovich-Danchenko, L. Y.; Lipnitski, A. G.; Kulkova, S. E. *Phys. Solid State* **2007**, *49* (6), 1079–1085.
- (36) Ledbetter, H. M. *Phys. Status Solidi A* **1981**, *66*, 477–484.
- (37) Ruiz, E.; Alvarez, S.; Alemany, P.; Evarestov, R. *Phys. Rev. B* **1997**, *56*, 7189–7196.
- (38) Nix, F. C.; MacNair, D. *Phys. Rev.* **1941**, *60*, 597–605.
- (39) Uno, R.; Okada, T. *J. Phys. Soc. Jpn.* **1950**, *5*, 23–25.
- (40) Zhang, X.; Shyy, W.; Sastry, A. M. *J. Electrochem. Soc.* **2007**, *154* (10), A910.
- (41) Rothman, S. J.; Peterson, N. L. *Phys. Status Solidi* **1969**, *35*, 305–312.
- (42) Mishin, Y.; Mehl, M. J.; Papaconstantopoulos, D. A.; Voter, A. F.; Kress, J. D. *Phys. Rev.* **2001**, *63*, 224106.
- (43) Andersson, D. A.; Simak, S. I. *Phys. Rev. B* **2004**, *70*, 115108.
- (44) Peterson, N. L.; Wiley, C. L. *J. Phys. Chem. Solids* **1984**, *45* (3), 281–294.
- (45) Bergsmark, E.; Simensen, C. J.; Kofstad, P. *Mater. Sci. Eng., A* **1989**, *120*, 91–95.
- (46) Campbell, T. J.; Kalia, R. K.; Nakano, A.; Vashishta, P.; Ogata, S.; Rodgers, S. *Phys. Rev. Lett.* **1999**, *82*, 4866–4869.
- (47) Henz, B. J.; Hawa, T.; Zachariah, M. R. *J. Appl. Phys.* **2010**, *107*, 024901.
- (48) Rai, A.; Park, K.; Zhou, L.; Zachariah, M. R. *Combust. Theory Modell.* **2006**, *10* (5), 843–859.
- (49) Zhanga, X.; Lu, G. *Phys. Rev. B* **2008**, *77*, 174102.
- (50) Lai, W. M.; Rubin, D.; Krempl, E. *Introduction to Continuum Mechanics*; Pergamon Press Ltd.: New York, 1993; p 291.
- (51) Fischer, F. D.; Svoboda, J. *Int. J. Solid Struct.* **2010**, *47* (20), 2799–2805.
- (52) Mei, Q. S.; Wang, S. C.; Cong, H. T.; Jin, Z. H.; Lu, K. *Acta Mater.* **2005**, *53*, 1059–1066.
- (53) Fan, H. J.; Knez, M.; Scholz, R.; Nielsch, K.; Pippel, E.; Hesse, D.; Zacharias, M.; Gosels, D. *Nat. Mater.* **2006**, *5*, 626–631.
- (54) Li, S.; Sellers, M. S.; Basaran, C.; Schultz, A. J.; Kofke, D. A. *Int. J. Mol. Sci.* **2009**, *10*, 2798–2808.

Comment on “Mechanochemical Continuum Modeling of Nanovoid Nucleation and Growth in Reacting Nanoparticles”

Vladimir P. Zhdanov*

Department of Applied Physics, Chalmers University of Technology, S-41296 Göteborg, Sweden
Boreskov Institute of Catalysis, Russian Academy of Sciences, Novosibirsk 630090, Russia

J. Phys. Chem. C **2012**, *116* (1), 54–62. DOI: 10.1021/jp2055365

J. Phys. Chem. C **2012**, *116*. DOI: 10.1021/jp3038472

Oxidation of metal nanoparticles is of high interest from very different perspectives. One of the unusual specifics of this process is that it is sometimes accompanied by the formation of hollows (voids) as schematically shown in Figure 1 (reviewed by Fan et al.¹). The understanding of the

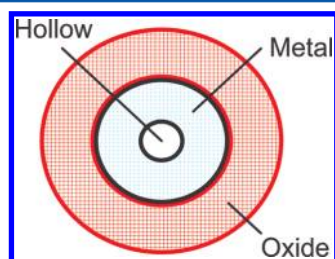


Figure 1. Schematic structure of a metal nanoparticle during oxidation.

mechanism(s) of this phenomenon is still limited. Specifically, the role of the lattice strain remains to be open for debate. The experiments indicate that the oxidation starts on the surface of a particle and results in the formation of an oxide shell. Due to material mismatch and expansion of the shell, the metal core is expected to be under tensile strain. Our analysis² (as well as refs 3 and 4) indicates that this strain may induce or facilitate the formation of a hollow. In a more recent analysis, Levitas and Attariani (LA)⁵ claim that this strain is negligible and focus their attention on the compressive strain related to surface tension. To discredit our work (and ref 3) and validate their model, LA refer to the experiments by Mei et al.⁶ (ref S2 in the quotation):

“... because in our problem the reaction occurs at the surface (rather than in the bulk) and the interface between the metal and oxide is incoherent, internal stresses due to chemical reaction are negligible. For example, an aluminum oxide shell is amorphous below some thickness (4 nm), and thus, the interface is incoherent and does not generate internal stresses. Even for a crystalline shell, for Al particles with $R_c = 20\text{--}40$ nm and a shell growing during chemical reaction ..., lattice spacing in Al did not differ from that in the bulk sample,⁵² i.e., internal stresses are negligible.”

Our three comments on the LV work are as follows:

1. As noticed in our Letter,² the formation of hollows in metal nanoparticles is usually observed at mild conditions or, more specifically, at relatively low temperatures. In particular, we mentioned experimental data for six metals. The corresponding temperatures are: 295 K for

Al (Figure 3; ref 7); ≤ 520 K for Fe;⁸ ≤ 455 K^{9,10} and ≤ 473 K (Figure 1; ref 11) for Co; 573–673 K for Ni (Figures 1 and 2; ref 12); 323–373 K for Cu;^{7,13} and 423 K for Zn (Figure 3; ref 14).

2. Mei et al.⁶ studied oxidation of three Al samples (see their Table 1). The corresponding temperatures and durations of experiments were: (A) 773 K/3 h + 873 K/1 h, (B) 773 K/3 h + 873 K/3 h, and (C) 773 K/3 h + 873 K/6 h. These temperatures are much higher than those in item 1 (especially for Al). Under such high temperatures, the stress could easily relax due to very rapid diffusion. For this reason, the fact that according to ref 6 the Al lattice expansion is negligible is, strictly speaking, irrelevant if one is interested in hollow formation.
3. In their model, LA postulate that the vacancies form a hollow in the center of a nanoparticle. If the oxide shell is amorphous so that the corresponding lattice strain is negligible as assumed by LA, one can wonder why the vacancies do not annihilate on the oxide/metal interface.

In summary, the LA criticism of our work is too categorical because the only reference they present is irrelevant. Their own model does not seem to be self-consistent.

AUTHOR INFORMATION

Corresponding Author

*E-mail: zhdanov@catalysis.ru.

Notes

The authors declare no competing financial interest.

REFERENCES

- (1) Fan, H. J.; Gösele, U.; Zacharias, M. *Small* **2007**, *3*, 1660–1671.
- (2) Zhdanov, V. P.; Kasemo, B. *Nano Lett.* **2009**, *9*, 2173–2176.
- (3) Svoboda, J.; Fischer, F. D.; Vollath, D. *Acta Mater.* **2009**, *57*, 1912–1919.
- (4) Svoboda, J.; Fischer, F. D. *Acta Mater.* **2012**, *59*, 61–67.
- (5) Levitas, V. I.; Attariani, H. *J. Phys. Chem. C* **2012**, *116*, 54–62.
- (6) Mei, Q. S.; Wang, S. C.; Cong, H. T.; Jin, Z. H.; Lu, K. *Acta Mater.* **2005**, *53*, 1059–1066.
- (7) Nakamura, R.; Tokozakura, D.; Nakajima, H.; Lee, J. G.; Mori, H. *J. Appl. Phys.* **2007**, *101*, 074303.

Received: March 24, 2012

Published: May 24, 2012

- (8) Cabot, A.; Puentes, V. F.; Shevchenko, E.; Yin, Y.; Balcells, L.; Marcus, M. A.; Hughes, S. M.; Alivisatos, A. P. *J. Am. Chem. Soc.* **2007**, *129*, 10358–10360.
- (9) Yin, Y.; Rioux, R. M.; Erdonmez, C. K.; Hughes, S.; Somorjai, G. A.; Alivisatos, A. P. *Science* **2004**, *304*, 711–714.
- (10) Yin, Y.; Erdonmez, C. K.; Cabot, A.; Hughes, S.; Alivisatos, A. P. *Adv. Funct. Mater.* **2006**, *16*, 1389–1399.
- (11) Chernavskii, P. A.; Pankina, G. V.; Zaikovskii, V. I.; Peskov, N. V.; Afanasiev, P. *J. Phys. Chem. C* **2008**, *112*, 9573–9578.
- (12) Nakamura, R.; Lee, J. G.; Mori, H.; Nakajima, H. *Philos. Mag.* **2008**, *88*, 257–264.
- (13) Tokozakura, D.; Nakamura, R.; Nakajima, H.; Lee, J. G.; Mori, H. *J. Mater. Res.* **2007**, *22*, 2930–2935.
- (14) Nakamura, R.; Lee, J. G.; Tokozakura, D.; Mori, H.; Nakajima, H. *Mater. Lett.* **2007**, *61*, 1060–1063.

Reply to "Comment on 'Mechanochemical Continuum Modeling of Nanovoid Nucleation and Growth in Reacting Nanoparticles'"

Valery I. Levitas^{*,†,‡,§} and Hamed Attariani[‡]

[†]Department of Aerospace Engineering, [‡]Department of Mechanical Engineering, and [§]Department of Material Science and Engineering, Iowa State University, Ames, Iowa 50011, United States

J. Phys. Chem. C **2012**, *116* (1), 54–62. DOI: 10.1021/jp2055365

J. Phys. Chem. C **2012**, *116*. DOI: 10.1021/jp302819x

The problem of the mechanisms of void nucleation in nanoparticles and related problem of the stresses and their relaxation in nanoparticles are of significant importance and far from being resolved. It is not surprising that there are several approaches with different and, in the given case, opposite assumptions. Thus, in ref 1, surface tension is neglected, and volumetric strain due to oxidation is introduced in the oxide shell. It is stated that for linear lattice mismatch $\alpha \geq 0.3$ large tensile stresses in a metal core are sufficient for void nucleation.

1. Let us estimate radial stress in a metal core required for void nucleation according to eq 14 in ref 1

$$\sigma_{rr} = \frac{2\alpha E}{3(1-\sigma)} \left(1 - \frac{R^3}{R_m^3} \right) \quad (1)$$

where E , σ , R , R_m , and α are the Young modulus, Poisson's ratio, core radius, radius of bare particle, and linear mismatch parameter, respectively. Taking $E = 100$ GPa, $\sigma = 0.3$, and neglecting $(R/R_m)^3$ to get the higher stresses required for nucleation, the authors¹ found that void can nucleate at $\alpha = 0.3$. Substituting these parameters in eq 1, one obtains that the tensile radial stress necessary for void nucleation is $\sigma_{rr} = 28.6$ GPa, which is much above the theoretical strength. For Cu, the change in volume during oxidation is $J = V_{ox}/V_m = (1 + \alpha)^3 = 1.65$, where $\alpha = 0.18$. For one of the Cu particles that we consider in ref 2, the core radius was 9 nm, and the initial shell thickness was 2.5 nm. Since void nucleation occurs at the very initial stage of oxidation, we determine for these parameters that $R = 9$ and $R_m = 10.63$ nm (R_m is obtained based on eq A.5 in the Appendix). Substitution of these values in eq 1 along with $E = 128$ GPa and $\sigma = 0.34$ gives $\sigma_{rr} = 9.15$ GPa, which is 2.93 times smaller than that required for void nucleation. Since stress contributes as a factor of σ_{rr}^{-4} to the activation energy, reduction in σ_{rr} by a factor of 2.93 increases activation energy by a factor of 73.7, which makes nucleation completely unrealistic. For Cu particles with a core radius of 15.9 nm and shell thickness of 2.5 nm in ref 2 ($R = 15.9$ nm, $R_m = 17.48$ nm), the radial stress is 5.76 GPa which increases the activation energy by a factor of 468.65. For Al, $J = 1.25$ and $\alpha = 0.077$, which with $E = 70$ GPa and $\sigma = 0.35$ results in $\sigma_{rr} = 5.53$ GPa even for neglected $(R/R_m)^3$ and increases activation energy by a factor of 551.62.

In addition, the required stress of 28.6 GPa causes volumetric expansion of 0.2. Such an expansion and $\alpha = 0.3$ are significantly above the range of applicability of the linear elasticity theory and eq 1. When elastic nonlinearity is taken into account, one needs even larger α to obtain the same

stresses. And finally, the size of a critical void in ref 1 at $\alpha = 0.3$ is 0.16 nm, which is less than the radius of a vacancy in Cu of 0.199 nm.³ Why does one need all these troubles with unrealistically large tensile stresses, when we just can introduce a single vacancy?

Since one of us recently published a number of papers on nanovoid nucleation under tensile stresses due to fracture, sublimation, sublimation via virtual melting, and evaporation,^{4–6} based on a similar kinetic approach like in ref 1 but with allowing for plasticity, large strains, and surface tension, we also applied a similar approach to void nucleation in reacting nanoparticles, based on more advanced equations than in ref 1. However, due to the above reasons, we decided that this scenario is completely unrealistic. We did not want to discredit ref 1, which is why we did not include our numerical estimates in ref 2, but now we are forced to do this.

2. Does change in volume due to chemical reaction cause large tensile stresses in a core of a nanoparticle and compressive stresses in a shell or do they relax? Note that at the nanoscale diffusion coefficients are much higher; see some data in ref 2. Even at the low temperature mentioned in ref 7, diffusion was fast enough to transport the entire metallic core outside the initial shell. Such fast diffusion at the time scale of oxidation can cause stress relaxation during chemical reaction, similar to that observed in ref 8 at higher temperature.

Traditional technologies for passivation of Al particles consist of holding synthesized bare nanoparticles at room temperature in oxygen or air. Thus, if we include volumetric transformation strain and neglect stress relaxation, the core of all nanoparticles should be under high tensile pressure, estimated by eq 1. Thus, we obtain for Al nanoparticles ($\alpha = 0.077$, $E = 70$ GPa, $\sigma = 0.35$, and $R = 50$ nm) that $\sigma_{rr} = 0.61$ GPa for $R_m = 52$ nm and $\sigma_{rr} = 1.14$ GPa for $R_m = 54$ nm. Such stresses should be easily detected by X-ray; however, in ref 8 lattice parameters at room temperature were the same for bulk Al and nanoparticles with different R and R_m . In ref 9, linear compressive strain of 0.017 was detected, which corresponds to an internal compressive pressure of 3.84 GPa in a core.¹⁰ Also, as was mentioned in ref 10, thermal stresses during heating of particles with different R/R_m should be different (see eq 1 in which alpha should be substituted with difference in thermal strains of a metal and a core). However, lattice spacing for samples with different M in ref 8 does not show any appreciable difference between room

Received: April 20, 2012

Published: May 24, 2012

temperature and 860 K, which means that internal stresses relax even at low temperature.

Also, one of the methods to increase the reactivity of nanoparticle suggested in refs 11 and 12 was based on the increase in temperature T_0 at which the particle is stress free. It was assumed that for purchased particles $T_0 = 298$ K, because this was their passivation temperature and based on data from ref 8, that lattice spacing for nanoparticles is the same as that of bulk Al. Prestressing was produced by heating particles to several elevated temperatures, holding them at a temperature for 10 min to relax thermal stresses, and cooling them at several rates to room temperature. For the optimal thermal treatment conditions (heating to 378 K and cooling at 0.13 K/s), the flame propagation speed increased by 31% for nanoparticles and 41% for micrometer particles, which was quantitatively consistent with theoretical predictions. Cooling at 0.06 K/s did not change the flame rate, which was explained by the slower cooling rate which allowed thermal stresses to relax during cooling. Change in stress-free temperature T_0 from 298 to 378 K induced at room temperature the thermal tensile radial stress in a core of 0.04 GPa and compressive hoop stress in a shell of 0.74 GPa, which suppressed fracture of the oxide shell, as desired. These results indirectly demonstrate that internal stresses may relax at temperatures as low as in the case for nanovoid nucleation and during a similar time range.

3. The main reason why internal stresses are strongly overestimated when eq 1 is applied is not related to stress relaxation due to diffusion only. The main reason is that the volumetric expansion due to reaction is applied in eq 1 isotropically, i.e., equally in all three directions, considering this transformation strain tensor as a spherical one. In reality, the expansion may occur anisotropically, driven by reduction in internal stresses. Indeed, if the entire expansion in the shell will occur in radial direction, no internal stresses will appear at all. At the macroscale, the anisotropic transformation strain tensor was measured for NiAl and Zr,^{13,14} and the ratio of a strain normal to an interface, ε_n , to a strain along the interface, ε_t , was $\varepsilon_n/\varepsilon_t = 87$ and 108. Thus, actual mismatch along the interface is approximately 2 orders of magnitude smaller than α . Similar anisotropic transformation strain was discussed in ref 15 for crystallization of amorphous alumina and in ref 16 for a phase field approach to melting. Later, in ref 17, the kinetic equation was derived that determines the deviatoric part of the transformation strain tensor for melting. We are working on a similar approach for oxidation now. Thus, we do not claim that change in volume due to chemical reaction does not produce internal stresses. However, they are 2 orders of magnitude lower than predicted by eq 1 (or more advanced eqs 40 and 41 in ref 2). That is why it was more accurate to ignore them, when we formulated and solved the problem on nanovoid nucleation and growth, than to introduce them as an isotropic mismatch strain.

4. Concerning our assumption that vacancies form a hollow at the center of a particle, why do vacancies not annihilate at the metal–amorphous oxide interface? An amorphous interface is observed for Al for interface width below 4 nm.¹⁸ For Cu, we did not find references that the interface is amorphous. We stated in ref 2 that while often multiple voids nucleate near the core/shell interface^{19,20} we placed the void at the center to obtain a simple, one-dimensional model, similar to all previous works. Very little is known about the structure of the metal–amorphous oxide interface for a nanoparticle during oxidation to claim that it serves as a sink for vacancies. In molecular

dynamic simulations²¹ for Ni–Zr core–shell structure, vacancies nucleated at the incoherent Ni–Zr interface then diffused into the core and formed a void. Due to mixing, the Ni–Zr shell undergoes amorphization, which does not prevent void growth due to generation of new vacancies. Thus, we do not see why the assumption that in some cases the shell is amorphous and interface is incoherent would make our model not self-consistent.

APPENDIX

To make an estimate of the stress according to eq 1, we need to determine the initial radius R_m of a bare particle that transforms to the core–shell structure with the prescribed oxide shell thickness t and corresponding volume $V_{ox} = 4\pi/3 ((R+t)^3 - R^3)$. This can be done by utilizing the mass balance. For the oxide shell with a volume V_{ox} and mass density ρ_{ox} , the oxide mass, m_{ox} , is

$$m_{ox} = n_m M_m + \frac{y}{x} n_m M_O = \rho_{ox} V_{ox} \quad (\text{A.1})$$

where n_m is the number of moles of a metal; M_m and M_O are the molar masses of a metal and oxygen; and y and x are the stoichiometric coefficients of an oxide M_xO_y . From eq A.1, the number of moles of metal in the oxide shell can be calculated as

$$n_m = \rho_{ox} V_{ox} / \left(M_m + \frac{y}{x} M_O \right) \quad (\text{A.2})$$

Therefore, the volume of the reacted metal, V_r , that produced volume of an oxide V_{ox} is

$$V_r = \frac{n_m M_m}{\rho_m} = \frac{\rho_{ox} M_m V_{ox}}{\rho_m \left(M_m + \frac{y}{x} M_O \right)} \quad (\text{A.3})$$

where ρ_m is the mass density of a metal. For a spherical particle, V_r can be written as

$$V_r = \frac{4\pi}{3} (R_m^3 - R^3) \quad (\text{A.4})$$

By equating eqs A.3 and A.4, the radius of the bare nanoparticle is

$$R_m = \left(\frac{3\rho_{ox} M_m V_{ox}}{4\pi\rho_m \left(M_m + \frac{y}{x} M_O \right)} + R^3 \right)^{1/3} \quad (\text{A.5})$$

In calculations, we used $M_m = 63.55$ g/mol, $M_O = 16$ g/mol, $\rho_m = 8.94$ g/cm³, $\rho_{ox} = 6$ g/cm³, $x = 2$, and $y = 1$.

AUTHOR INFORMATION

Corresponding Author

*E-mail: vlevitas@iastate.edu.

Notes

The authors declare no competing financial interest.

REFERENCES

- (1) Zhdanov, V. P.; Kasemo, B. *Nano Lett.* **2009**, *9* (5), 2172–2176.
- (2) Levitas, V. I.; Attariani, H. *J. Phys. Chem. C.* **2012**, *116* (1), 54–62.
- (3) Nemirovich-Danchenko, L. Y.; Lipnitski, A. G.; Kulkova, S. E. *Phys. Solid State* **2007**, *49* (6), 1079–1085.
- (4) Levitas, V. I.; Altukhova, N. *Phys. Rev. Lett.* **2008**, *101* (14), 145703.
- (5) Levitas, V. I.; Altukhova, N. *Phys. Rev. B* **2009**, *79* (21), 212101.

- (6) Levitas, V. I.; Altukhova, N. *Acta Mater.* **2011**, *59* (18), 7051.
- (7) Zhdanov, V. P. Comment on "Mechanochemical Continuum Modeling of Nanovoid Nucleation and Growth in Reacting Nanoparticles". *J. Phys. Chem. C* **2012**, DOI: 10.1021/jp302819x.
- (8) Mei, Q. S.; Wang, S. C.; Cong, H. T.; Jin, Z. H.; Lu, K. *Acta Mater.* **2005**, *53*, 1059–1066.
- (9) Ramaswamy, A. L.; Kaste, P. *J. Energy Mater.* **2005**, *23*, 1.
- (10) Levitas, V. I.; Pantoya, M.; Chauhan, G.; Rivero, I. *J. Phys. Chem. C* **2009**, *113* (32), 14088–14096.
- (11) Levitas, V. I.; Asay, B. W.; Son, S. F.; Pantoya, M. *J. Appl. Phys.* **2007**, *101*, 083524.
- (12) Levitas, V. I.; Dikici, B.; Pantoya, M. *Combust. Flame* **2011**, *158*, 1413–1417.
- (13) Huntz, A. M.; Amiri, G.; Evans, H. E.; Cailletaud, G. *Oxid. Met.* **2002**, *57*, 499.
- (14) Parise, M.; Sicardy, O.; Cailletaud, G. *J. Nucl. Mater.* **1998**, *256*, 35.
- (15) Watson, K. W.; Pantoya, M.; Levitas, V. I. *Combust. Flame* **2008**, *155*, 619–634.
- (16) Levitas, V. I.; Samani, K. *Nat. Commun.* **2011**, *2*, 284.
- (17) Levitas, V. I.; Samani, K. *Phys. Rev. B. Rapid Commun.* **2011**, *84* (14), 140103(R).
- (18) Jeurgens, L. P. H.; Sloof, W. G.; Tichelaar, F. D.; Mittemeijer, E. *J. J. Appl. Phys.* **2002**, *92* (3), 1649.
- (19) Wang, C. M.; Baer, D. R.; Thomas, L. E.; Amonette, J. E.; Antony, J.; Qiang, Y.; Duscher, G. *J. Appl. Phys.* **2005**, *98*, 094308.
- (20) Railsback, J. G.; Johnston-Peck, A. C.; Wang, J. W.; Tracy, J. B. *ACS Nano* **2010**, *4* (4), 1913–1920.
- (21) Delogu, F. *Mater. Chem. Phys.* **2011**, *125*, 390–396.